

# Cross Comparison of EO-1 Sensors and Other Earth Resources Sensors to Landsat-7 ETM+ Using Railroad Valley Playa

Kurtis J. Thome, Stuart F. Biggar, and Wit Wisniewski

**Abstract**—The Remote Sensing Group at the University of Arizona has used ground-based test sites for the vicarious calibration of airborne and satellite-based sensors, of which the Railroad Valley Playa in north central Nevada has played a key role. This work presents a cross comparison of five satellite-based sensors that all imaged this playa on July 16, 2001. These sensors include the Advanced Land Imager and Hyperion on the Earth Observer-1 platform, the Landsat-7 Enhanced Thematic Mapper Plus (ETM+), Terra's Moderate Resolution Imaging Spectroradiometer, and Space Imaging's Ikonos. The approach atmospherically corrects the ETM+ data to derive surface reflectance for a 1 km × 1 km area of the playa and then uses these reflectances to determine a hyperspectral at-sensor radiance for each of the sensors taking into account the changes in solar zenith angle due to any temporal differences in the overpass times as well as differences in the view angles between the sensors. Results show that all of the sensors agree with ETM+ to within 10% in the solar reflective for bands not affected by atmospheric absorption. ETM+, MODIS, and ALI agree in all bands to better than 4.4% with better agreement in the visible and near infrared. Poorer agreement between Hyperion and other sensors appears to be due partially to poorer signal to noise ratio in the narrowband Hyperion datasets.

**Index Terms**—Absolute-radiometric calibration, atmospheric correction, vicarious calibration.

## I. INTRODUCTION

THE Earth Observer-1 (EO-1) platform was launched onboard a Boeing Delta II launch vehicle in November 2000. The platform was placed in an orbit only 1 min behind the Landsat-7 platform, and approximately 40 min ahead of the Terra platform. The primary purpose of the EO-1 mission is to provide a technological testbed for spaceborne components. For example, the mission includes tests of an X-band phased array antenna (allowing for no moving parts to point the antenna at the receiving station), plasma-based ion thrusters (to provide platform maneuverability at low mass and low cost while eliminating liquid sloshing), and carbon-based mechanical structures (to reduce significantly the weight of the platform). The EO-1 platform has three sensors onboard, two of which, the Advanced Land Imager (ALI) and Hyperion, are discussed here. The ALI

provides multispectral data similar to that of the Enhanced Thematic Mapper Plus (ETM+) sensor on Landsat-7. Key differences between ETM+ and the ALI are that ALI is a pushbroom sensor as opposed to the whiskbroom design of ETM+, and there are several additional bands on ALI with respect to ETM+. These bands include a band at a wavelength shorter than that of band 1 of ETM+ to evaluate possible water quality applications and atmospheric studies, an additional band in the shortwave infrared between ETM+ bands 4 and 5 for possible improvements to surface classification studies, and a narrowband version of ETM+ band 4 to avoid water vapor absorption. While the added bands of ALI and the improved signal-to-noise ratio from the pushbroom approach are definite improvements over ETM+, a strong advantage to ETM+ is the presence of a thermal band. The Hyperion sensor, on the other hand, has no comparable sensor in earth orbit. It is the first instance of a grating-based, hyperspectral, civilian sensor in earth orbit.

As mentioned above, a critical component to the EO-1 project is technological evaluations. One aspect of this technical evaluation is to determine whether this new technology can provide radiometric performance on par with or better than other current sensors. One approach to evaluate the radiometric performance is to compare the output from the sensor under study to that of a well-understood system. The near-coincidence of the EO-1, Landsat-7, and Terra platforms allows this comparison approach to be used between ALI, Hyperion, ETM+, the Advanced Spaceborne Thermal Infrared Emission and Reflection Radiometer (ASTER), the Multi-angle Imaging Spectroradiometer (MISR), and Moderate Resolution Imaging Spectroradiometer (MODIS) sensors. These comparisons can be made between ALI and Hyperion whenever these two sensors are operated because the 100% duty cycle of MODIS, MISR, and ETM+ sensors over the United States would allow comparisons of any ALI/Hyperion acquisitions over the United States.

The approach presented here relies on ground-based measurements of atmospheric and surface properties at a well-understood ground site in central Nevada. The Remote Sensing Group (RSG) of the Optical Sciences Center at the University of Arizona has used this site since 1996 for the radiometric calibration of satellite and airborne sensors in the solar reflective. This approach to radiometric calibration, often referred to as vicarious calibration or radiance validation, relies on understanding the atmosphere over a test site and the reflectance characteristics of that site at the time of sensor overpass. This information can be obtained either through ground-based measurements or

Manuscript received July 17, 2002; revised March 24, 2003. This work was supported by the National Aeronautics and Space Administration (NASA) under Contract NAS5-31717, by NASA Grant NAG5-2448, and by the Commercial Data Buy Program at Stennis Space Center.

The authors are with the Remote Sensing Group, Optical Sciences Center, University of Arizona, Tucson AZ 85721 USA.

Digital Object Identifier 10.1109/TGRS.2003.813210

through cross-calibration/comparison methods [1]–[9]. The current work focuses on a cross-comparison approach that allows data from ETM+ to be used for the radiance validation of the EO-1 sensors. In a cross-comparison approach, the calibration from a well-understood sensor (ETM+ in this case) is effectively transferred to another sensor [9]. For best results, a large uniform area is imaged simultaneously, or nearly so, by the two sensors with similar view angles.

As already mentioned, ETM+ and MODIS data are used here for comparison to the ALI and Hyperion data. In addition, data from Space Imaging's Ikonos sensor are also used. ETM+ is selected as the base reference because it has been shown, based on onboard and vicarious approaches, to be stable to better than 2% since its April 1999 launch. Also, the absolute radiometric calibration is known to better than 3% [10]–[12] and its 30-m spatial resolution for the multispectral reflective bands allows the location of ground-based measurements to be easily found in the imagery. Additionally, ETM+ covers the same spectral range as all of the other sensors, and it has the "same" orbit as the EO-1 (within 1 min) platform. Thus, Ikonos is not a desired reference due to the lack of bands at wavelengths longer than 1.0  $\mu\text{m}$ . ALI and Hyperion, both have 30-m spatial resolution and cover the desired spectral regions, but neither has the proven history of calibration that ETM+ has.

The other two sensors (MODIS and Ikonos) are dramatically different in spatial resolution from ALI, ETM+, and Hyperion. MODIS, one of five sensors onboard the Terra platform (launched December 1999) has spatial resolutions of 250, 500, and 1000 m depending on the spectral band. MODIS, along with ETM+, is an important part of NASA's Earth Observing System (EOS) [13]. The number of bands for MODIS and the varying spatial characteristics makes it a challenge from a radiometric calibration standpoint. Because radiometric characterization is a critical element of MODIS and EOS [13], the onboard radiometric calibration of MODIS includes multiple approaches so as to provide several independent methods of calibration to evaluate MODIS [14]. Space Imaging's Ikonos sensor is on a dedicated platform and is at the other end of the spatial resolution scale being the first high-spatial resolution (better than 1-m panchromatic) commercial imager in space. It has four multispectral bands similar to the first four bands of ETM+ but with a spatial resolution of 4 m. The data used here were acquired through NASA's Science Data Buy based at the Stennis Space Center. No data from ASTER or MISR are included here for simplicity. The approach presented here can be readily applied to these sensors as data become available.

Section II describes the Railroad Valley test site followed by a description of how this site is used in the cross-comparison approach. Briefly, the method uses atmospherically corrected ETM+ data to derive an estimate of the surface reflectance of a 1 km  $\times$  1 km area. This derived surface reflectance is then used in a radiative transfer code to predict at-sensor radiance for 1-nm intervals from 350–2500 nm. This predicted radiance is produced for the specific sun-view geometry for each sensor and is then band averaged based on the spectral response of each sensor to produce in-band radiance for each sensor. This approach produces results for a cross comparison of ETM+ to itself to better than 2% in all bands and better than 5% in all

bands of all sensors except bands 2 and 3 of Ikonos and several Hyperion bands affected by atmospheric absorption.

## II. RAILROAD VALLEY TEST SITE

The Railroad Valley test site used in this work is located in central Nevada between the towns of Ely and Tonopah and is a 14-h drive from the RSG's laboratory in Tucson. The overall size of the playa is approximately 15 km  $\times$  15 km, and it is located at an elevation of approximately 1.5 km in a geographical region with reasonably high expectations of clear weather and typically low levels of aerosol loading. The central area of the playa is flat to better than 100 m; however, this relative flatness causes problems in that low areas to the north will collect standing water of several centimeters over a horizontal extent in excess of 200 m. Ground-based atmospheric measurements since 1999 by the RSG have been made at a latitude and longitude of 38.504 N and 115.692 W. Between 1996 and 1999, several sites were tested for their logistical and spatial homogeneity properties but have been rejected in favor of the current site. The test site that the RSG uses for the reflectance-based calibration of sensors with spatial resolutions of 50 m or less is located approximately 100 m to the east of this location and has been used consistently since 1999. The center of the 1 km  $\times$  1 km area used for the cross-calibration work is located at 38.497 N and 115.691 W, approximately 700 m south of the atmospheric instrumentation, and has been measured consistently since 2000.

Typical atmospheric conditions at the site include an aerosol optical depth at 550 nm that is less than 0.05 and horizontal visibilities in excess of 60 km. Measurements of atmospheric aerosols using solar radiometer techniques show that the horizontal variability of the aerosols varies on the order of the noise of the measurements on a typical day. This is inferred by operating two sensors at separate locations on the playa as well as collecting data over time. However, aerosols can vary dramatically across the playa on dates for which clouds are present and for dates for which there are extreme wind conditions. These wind conditions will create blowing dust that quickly settles once wind conditions decrease.

Peak precipitation occurs in winter between December and March and during the summer months of July and August. Precipitation in winter falls as both rain and snow and is due mostly to large-scale weather systems moving across the state of Nevada. Summertime rainfall is caused primarily by isolated shower activity that can produce locally heavy rainfall. In addition to rainfall patterns, there is a higher probability of general cloud cover from November to April caused again by large-scale weather patterns moving across the area. There is also an additional feature to the Railroad Valley site that is not seen at other test sites used by the RSG. This is the large number of aircraft contrails that can form and then dominate the sky in conditions that might normally have clear skies or very thin cirrus conditions. The contrails are a result of the large amount of commercial air traffic traveling to and from the west coast across this area as they are forced north by several military air space restrictions.

The reflectance of this 1-km<sup>2</sup> site, and other regions near the center of the playa, is generally greater than 0.3 and relatively flat spectrally except for the blue portion of the spectrum and an absorption feature in the shortwave infrared (an example of the spectral reflectance can be seen in Fig. 3). Ideally, this reflectance would be constant throughout the year, but experience with this site shows that there are significant changes in reflectance with changes in surface moisture. These effects occur primarily in the winter months from the large-scale weather systems and the periodic episodes of heavy rain during summer. Ground-based measurements of the directional reflectance characteristics of the playa show it to be nearly Lambertian out to view angles of 30° for incident solar zenith angles seen for overpasses of EO-1, Ikonos, Terra, and Landsat-7. All of these factors are critical to reducing the uncertainties of a cross-calibration method [15].

In addition to the directional and spectral reflectance qualities of the surface, spatial uniformity is especially important since it minimizes the effects of misregistrations between the sensors being cross-compared. Past work to evaluate the suitability of the Railroad Valley site for cross calibration showed that the effects of misregistration is generally less than 0.5% for the worst case of a 500-m misregistration (possible between MODIS and the other sensors) of the selected area of Railroad Valley. The effect due to misregistration is largest in band 7 of ETM+ with a value of 2.0%. The smallest differences are seen with misregistration in the east–west direction, with a larger difference in the north–south direction with regions to the north of the playa area being darker than areas to the south [16].

Logistically, the site has several properties of interest. Ground-based measurements of surface reflectance are made more difficult by the fact that the surface has a soft, spongy character. This makes carrying equipment more difficult, much like walking on sandy beach, than at other sites used by the RSG where the ground is much harder. This soft surface also has the disadvantage that personnel walking on the site break the upper crust of the surface revealing a darker subsurface. The footpaths caused by personnel persist over long periods of time with rainfall leading to renewing the reflectance of the ground in the footprints, but wind erosion is the primary mechanism for returning the surface to its original state. At the writing of this paper, footpaths created in 2001 that have not been walked along since are still visible in 2003. This feature of the surface has altered somewhat the philosophy of the RSG's data collections, but primarily affects the calibration of ultra-high resolution sensors such as Ikonos. An additional logistical consideration is site access. This is obtained via gravel roads that are controlled by the Bureau of Land Management (as is the entire Railroad Valley Playa). There are several locations on this road that are suitable for locating vehicles and the RSG's mobile laboratory. This was one of the reasons for the use of two separate sites: one for high-resolution sensors and the other for low-resolution sensors.

### III. CROSS-CALIBRATION APPROACH

The typical method used by the RSG for high-spatial-resolution sensors is the reflectance-based approach in which

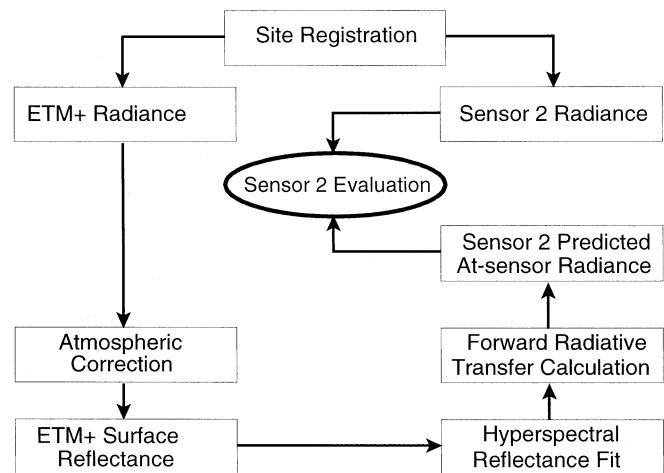


Fig. 1.

ground-based measurements of surface reflectance and atmospheric properties are used in a radiative transfer model to predict an at-sensor radiance [5], [6]. This approach has been applied to all of the sensors in this work. The cross-comparison approach used here is effectively the same as the reflectance-based. The goal is to derive the surface reflectance for the 1-km<sup>2</sup> area and using this reflectance as an input to a radiative transfer code, along with the coincident atmospheric data, allows a prediction of the at-sensor radiance. The key difference is that rather than basing the surface reflectance on ground-based measurements, the surface reflectance is derived from ETM+ data. The data used in this work is the Level 1G ETM+ product which has been both radiometrically and geometrically corrected. Fig. 1 illustrates this approach. Philosophically, the approach is similar to that described by Teillet *et al.* [17].

The first step in the calibration process is to select the test site common to the two sensors. Ideally, the data from both sensors would be coincident in time with identical view and solar geometries. Fortunately, the near-coincidence in view geometry and only 40 min being the largest separation in time between any two sensors leads to minimal uncertainties for the Railroad Valley test site. The specific area of the playa described in the last section corresponds approximately to a 33 × 33 pixel region of ETM+. A simple arithmetic average is used to derive the digital counts of the site that are converted to radiance using the prelaunch calibration coefficients.

Once the at-sensor radiance in all spectral bands for ETM+ is determined, an atmospheric correction is applied to the data to determine a surface reflectance for the 1-km<sup>2</sup> area. The correction relies on data from ground-based solar radiometer measurements operated at the time of the overpass of ETM+ [18]. Spectral optical depths derived from the solar radiometer data are inverted to determine column ozone, column water vapor, and aerosol size distribution [19]–[21]. The results from the atmospheric retrieval are input to a Gauss–Seidel radiative transfer code for two assumed surface reflectance values [22]. Fig. 2 shows the radiative transfer code results for bands 1 and 4 of ETM+ for data collected at Railroad Valley on July 16, 2001. Similar results are found for the other bands but are omitted

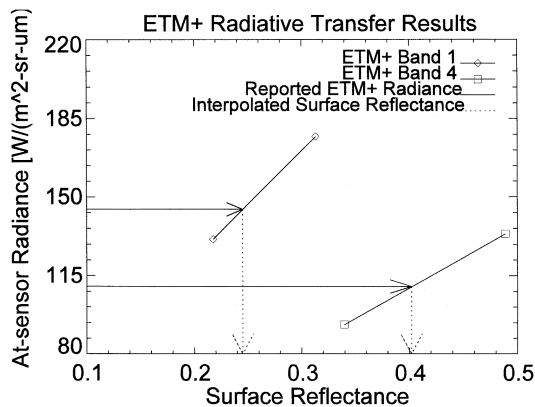


Fig. 2. Radiative transfer code results used to infer surface reflectance in ETM+ bands 1 and 4 based on reported radiance from ETM+.

for clarity. The endpoints of the two lines are the radiative transfer code results for the given atmospheric conditions and assumed surface reflectance values. Bands affected by strong gaseous absorption due to water vapor are corrected based on column-water vapor derived from the solar radiometer data and the radiative transfer code MODTRAN [23]. If it is assumed that the relationship between reflectance and at-sensor radiance is linear over the surface reflectance range shown, then knowing the at-sensor radiance allows the surface reflectance to be determined by linear interpolation. The values for the at-sensor radiance determined from the ETM+ image are indicated by the horizontal solid line in the figure. These radiances lead to an interpolated value for a reflectance as given by the dotted line in Fig. 2. Examination of radiative transfer code results from several cases for the RSG's test site shows that the linear assumption leads to less than a 0.1% error in the retrieved reflectance for the typical conditions.

The surface reflectance derived from the atmospheric correction of ETM+ data are curve fit using the results of ground-based measurements of surface reflectance. This ground-based reflectance is obtained from an ASD FieldSpec FR referenced to a Spectralon® panel of known reflectance. The spatial location of these data correspond to the 80 m  $\times$  300-m test site used for higher spatial resolution sensors. The curve fit assumes that the shape of the surface reflectance for the 1-km<sup>2</sup> area matches identically that of the ground-based measurements and only the absolute value of the reflectance is not known due to the fact that the ground-based measurements do not coincide with the 1-km area of the ETM+ scene used for the cross comparison. The curve fit relies on a multiplicative factor that is altered until the minimum least squares sum of the difference between the ETM+-derived and the band-averaged surface reflectances is found (Fig. 3 shows the results of this approach for July 16, 2001).

At this stage in the process, a hyperspectral reflectance of the 1-km<sup>2</sup> area of the playa is known. Ideally, this reflectance would then be further modified to predict the reflectance for the sun-sensor geometry of each individual sensor using the bi-directional reflectance distribution function (BRDF). Fortunately, past work by the RSG at this site shows that there is less than a 2% deviation from Lambertian for view angles out to 30° and solar angles typical of this test site at the times of sensor over-

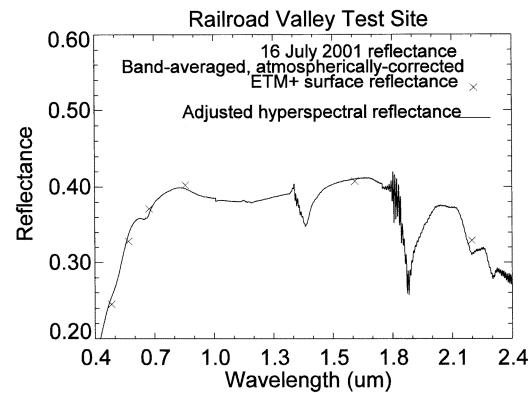


Fig. 3. Example of hyperspectral reflectance fit to retrieved from atmospherically corrected ETM+ surface reflectance.

pass. Thus, the surface reflectance is assumed constant for all overpasses and this reflectance is used as input to the radiative transfer code to predict at-sensor radiance for each sensor. This takes into account changes in atmospheric conditions, changes in atmospheric effects due to the specific sun-sensor geometry of each individual sensor, as well as effects due to the changing angle of the incident solar irradiance. The resulting at-sensor predictions of the radiance are band-averaged to give values valid for the specific spectral bands of each sensor. These predicted radiances are then compared to the reported radiance determined for each sensor for the 1-km area of the playa based on the appropriate calibration information.

#### IV. RESULTS

The above-described approach has been applied to data collected on July 16, 2001 at Railroad Valley. This date has the advantage of being a high sun angle case (low solar zenith) which further reduces any small effects due to BRDF as well as changes in at-sensor radiance due to differences in the incident solar zenith angle. The sun-sensor geometries for all sensors are listed in Table I. Ground-based measurements of atmospheric conditions exist for all overpasses and these are also summarized in Table I. The aerosol optical depths shown in the table are both an indication of the temporal stability of the atmosphere on this date as well as the low amount of aerosol loading. From the temporal stability of the aerosols, one can infer a spatial uniformity as well. A further example of the temporal stability is given in Fig. 4, which shows the derived aerosol optical thickness for the reference wavelength of 550 nm as a function of time for the 1-h period about the EO-1 overpass. The optical depth varies on the most part by less than 0.005 during the period, and this was also the case during the entire measurement period from near sunrise to local solar noon. The Junge parameter given in the table is an indication of the aerosol size distribution and this is also relatively constant. Fig. 5 shows how these Junge parameters are derived using a linear fit to the spectral optical depth corrected for molecular scattering. Deviation from the straight line around 600 and 940 nm are due to gaseous absorption. Other deviations from the fit are noise in the instrument and deviation from a Junge power law. From this plot, it is clear that the fit is not perfect. Fortunately, sensitivity analyses of the effect of errors in the Junge assumption and derivation

TABLE I  
SUMMARY OF ATMOSPHERIC AND SUN-VIEW GEOMETRY FROM JULY 16, 2001 AT RAILROAD VALLEY PLAYA FOR EACH OF THE SENSORS IN THE CURRENT STUDY

Sensor	ETM+	Hyperion/ALI	MODIS	Ikonos
Overpass Time (UTC)	18:10:25	18:11:19	18:46:37	18:48:22
Solar Zenith Angle (degrees)	27.3	27.1	21.8	21.5
Solar Azimuth Angle (degrees)	122	122	138	138
Sensor View Angle (degrees)	0.3	0.3	0.3	23.2
Sensor Azimuth Angle (degrees)	104	104	104	294
550 nm Aerosol Optical Depth	0.048	0.048	0.051	0.051
Junge Parameter	2.68	2.70	2.69	2.69
Column Ozone (cm-atm)	0.38	0.39	0.38	0.38
Column Water Vapor (cm)	0.99	0.99	1.04	1.04

of the column ozone show that the impact is less than 1% at all wavelengths. Columnar water vapor is also shown for each overpass and these values have uncertainties of 10%.

The atmospheric information for the ETM+ overpass were used to derive surface reflectance values for each of the ETM+ multispectral bands. These values are given in Table II. In the same table are the band-averaged values for the  $300 \text{ m} \times 80 \text{ m}$  area site for which the curve fit is based, the derived reflectance values for the  $1 \text{ km}^2$  and the measured surface reflectance for this same  $1\text{-km}^2$  area using a sampling scheme developed for the reflectance-based calibration of MODIS [24]. As can be seen from the table, the derived surface reflectance from the curve fit of the atmospherically corrected ETM+ data (row 2 of the Table II) agrees well with the measured surface reflectance of the  $1\text{-km}^2$  area (row four of the table). Differences between these two sets of reflectances are due to errors in the ground-based measurements, errors in the concept of the simple curve fit, small possible calibration biases in the ETM+ data, and uncertainties in the atmospheric correction approach. A brief assessment of the effect of these errors is given in the next section. What is clear from the table by examining rows three and four is that the uniformity of some areas of the playa at smaller scales is not sufficient to allow a set of ground-based measurements to be used for other unmeasured regions of the playa. The surface reflectance used in the subsequent processing to predicted at-sensor radiances are the hyperspectral values at 1-nm intervals that were used to derive the second row in Table II.

The derived surface reflectance values for the  $1\text{-km}^2$  area are used with the atmospheric properties and sensor specific geometries in Table I to give at-sensor radiances for each of the spectral bands for each sensor. These radiances are then compared with those reported by each sensor obtained by averaging the appropriate pixels of each image. Table III gives the values for each of the bands of ETM+. The first column of radiances are those derived from the ETM+ imagery, the subsequent columns are those radiances derived from the radiative transfer calculations for each of the atmospheric and geometry conditions of the other overpasses. Of note is the good agreement between the predicted and measured radiances for the ETM+ overpass. This indicates that there are no severe biases incurred from the atmospheric

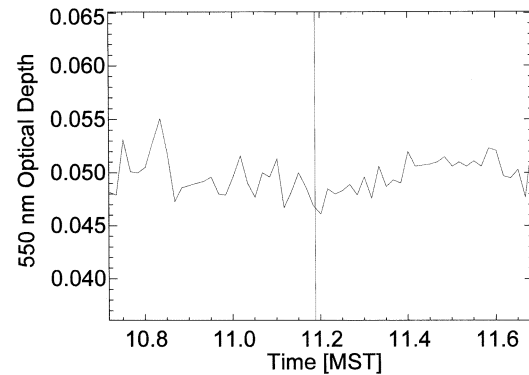


Fig. 4. Derived aerosol optical thickness at 550 nm with the overpass of EO1 indicated by the vertical line.

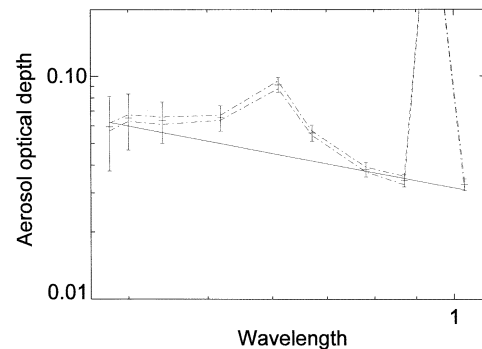


Fig. 5. Residual optical depth as a function of wavelength on In-In-scale showing the best fit Angstrom slope related to Junge parameter.

correction scheme and curve fit to the ground-based surface reflectance data. Note also that the level of agreement between the four predicted radiances corresponding to each of the overpasses shows that there is minimal change incurred due to differences in the overpass times. The largest difference is between the predictions for the Landsat-7 overpass time and geometry to that of the Terra overpass. Much of this difference is due to the difference in solar zenith angle changing the path length of the solar beam through the atmosphere (less attenuation of the direct solar irradiance) and an increase in the solar irradiance due to the smaller angle of incidence for the Terra case.

TABLE II  
SURFACE REFLECTANCE BASED ON ATMOSPHERICALLY CORRECTED ETM+ DATA, MEASURED  
GROUND-BASED DATA, AND PREDICTED VALUES FROM CURVE FIT

	Band 1	Band 2	Band 3	Band 4	Band 5	Band 7
Atmospherically-corrected ETM+	0.245	0.328	0.371	0.402	0.407	0.329
Modeled 1 km <sup>2</sup> area	0.254	0.332	0.367	0.396	0.409	0.330
Measured 80m by 300 m area	0.261	0.342	0.378	0.407	0.421	0.340
Measured 1 km <sup>2</sup> area	0.263	0.347	0.387	0.409	0.419	0.338

TABLE III  
PREDICTED RADIANCE FOR EACH ETM+ BAND AND EACH OVERPASS ALONG  
WITH REPORTED ETM+ RADIANCES FROM IMAGERY. ALL RADIANCES ARE IN  
UNITS OF WATTS PER SQUARE METER STERADIAN MICROMETER

	Reported	ETM+ overpass	EO-1 overpass	Terra overpass	Ikonos overpass
Band 1	144.5	148.9	148.9	155.2	151.8
Band 2	156.3	158.2	158.2	165.4	163.1
Band 3	148.4	146.8	146.8	153.4	152.1
Band 4	110.2	108.4	108.4	113.1	112.6
Band 5	23.97	24.07	24.07	25.12	25.08
Band 7	6.661	6.669	6.669	6.983	6.939

Fig. 6 shows the radiance as a function of wavelength reported by each sensor. Fig. 6(a) shows those values for the visible and near-infrared (NIR) portion of the spectrum while Fig. 6(b) shows the shortwave infrared. From this, it is clear that there are biases between the sensors that are larger than can be explained by changes in overpass times and view angles. These differences become clearer when the percent difference between the predicted and measured radiances are examined (see Fig. 7). In this case, the first key conclusion is that applying this cross-calibration approach to ETM+ using ETM+ as a reference gives differences less than 2% in all bands except band 1, which is 3%. This gives an indication of the level of uncertainty introduced by the curve fit approach to the spectral reflectance and indicates that the simplistic approach may require modification to ensure the best possible accuracy. Studies from hyperspectral imagery and more extensive ground-based measurements are planned to be studied to refine the curve fitting approach. A second item of note is that the multispectral systems of MODIS and ALI give results that agree to better than 5% in all bands and better than 3% in most bands. Hyperion data also agree in the visible and NIR to better than 5% for the most part, though data in the shortwave infrared have larger differences. The final sensor, Ikonos, shows agreement to better than 10% in all bands except band 3.

It should be pointed out that all of the results shown in Fig. 7 rely on the most recent understanding of the radiometric calibration of each sensor. For MODIS, this implies that a recent Level 1B dataset was received from the EOS Core System and calibration information provided in the metadata was used. This coefficient of MODIS relies on measurements of the onboard diffuser corrected for degradation using data from the solar-diffuser-sta-

bility monitor. The coefficients used to correct the Ikonos data are those supplied by Space Imaging for datasets provided after February 2001. ALI and Hyperion results depend upon calibration coefficients derived in December 2001. These coefficients included large corrections for bands 1p and 5 of ALI and an 8% correction for Hyperion in the VNIR and 18% in the SWIR [25]. The corrections for the EO-1 sensors were based on information from lunar views, the onboard solar diffusers, and vicarious calibrations using the reflectance-based approach. While Railroad Valley data from several dates (including July 16, 2001) were used to develop these new coefficients, the cross-comparison approach here is still independent of the earlier results.

## V. DISCUSSION OF UNCERTAINTIES

The sources of uncertainty in this approach can be viewed as three distinct areas: 1) surface reflectance, 2) atmospheric effects, and 3) misregistration of images. Uncertainties in the approach due to atmospheric conditions are minimized by the fact that the same radiative transfer code and assumptions are made for all predictions. Thus, any biases caused by the atmospheric corrections and radiative transfer calculations will cancel and uncertainties are primarily caused by changes in the atmosphere between overpasses. Of course, this assumes that the spectral response functions of the instruments are known to an accuracy such that effects at the wings of atmospheric absorption features do not dominate. The parameters related to atmospheric effects that can change between overpasses of the sensors being compared are the geometry between the sun and sensors, the amount of aerosols (optical depth), the aerosol type (size distribution, composition, and index of refraction), and amounts of gaseous absorbers (ozone and water vapor). In all cases, the precision in the derivation of the atmospheric parameters is far better than the absolute accuracy. Thus, while the uncertainty of the retrieved columnar water is 10%, the noise in the retrieval is less than 1%. The number of significant figures for the values of atmospheric parameters given in Table I for each of the overpass times indicate the level of precision expected for each parameter. While the values in the table have uncertainties such that the absolute value of the parameters could be in error, the differences in the table are real differences in the given parameter. As can be seen in Table I, these differences are extremely small. Radiative transfer simulations using the values in the table lead to a relative uncertainty in the radiative transfer predictions of much less than 1% in all bands.

In addition to atmospheric errors, the cross-comparison approach assumes that the same ground area can be found in the

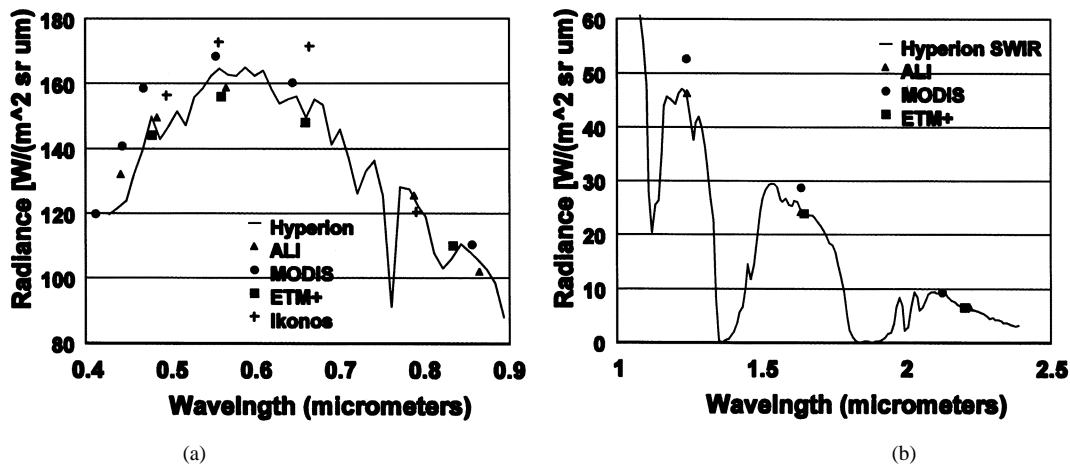


Fig. 6. Radiance as a function of wavelength reported by each sensor. (a) Values for the visible and NIR portion of the spectrum. (b) Shortwave infrared.

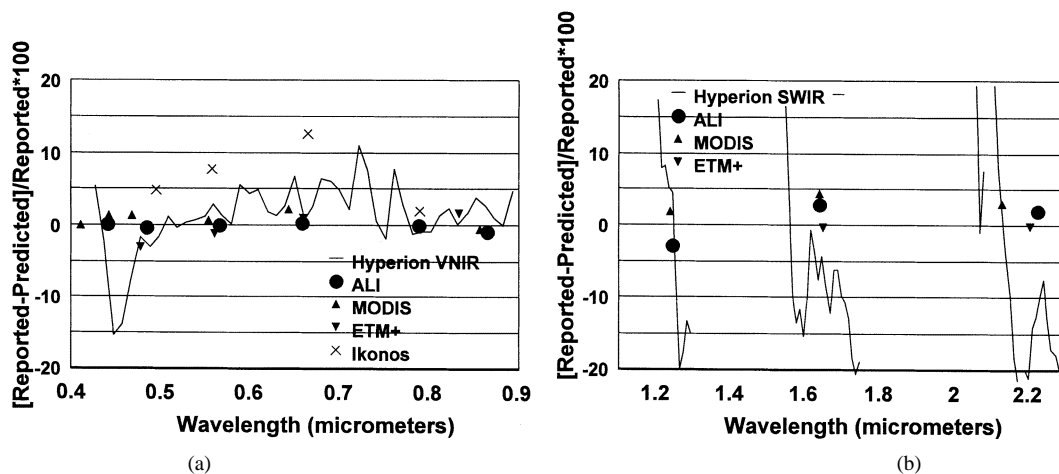


Fig. 7. Percent difference between the predicted and measured radiances for each sensor. (a) VNIR portion of the spectrum. (b) SWIR.

imagery of all of the sensors. The sensor output for this area is used to determine the at-sensor radiance and this radiance can be in error due to errors in sensor calibration and errors in locating the same area on the ground in all images. The error due to calibration is the purpose of the work described here. The error due to site location ambiguity is minimized since the method here relies on locating the center point of the 1-km<sup>2</sup> area rather than attempt to register the data from each sensor to every other sensor. The center point is readily found in all sensors with spatial resolution less than 30 m because of a graveled area alongside the access road that runs through the playa. Thus, the misregistration between ALI, ETM+, Hyperion, and Ikonos should be less than 60 m. The uncertainty due to this ambiguity is found to be < 0.1% based on selecting alternate 1-km<sup>2</sup> areas translated by 30 and 60 m in each of the cardinal directions (north, south, east, and west). In the case of MODIS, there are two uncertainties to consider related to site ambiguity. The first is that the wrong pixels are selected from the imagery. Examination of the adjacent pixels in the MODIS imagery show that using these pixels give differences less than 2.3% in the predicted at-sensor radiance in all bands with no consistent spectral dependence. The second cause of uncertainty is that the pixels that are selected in the MODIS imagery do not correspond to the same area as that used for the ETM+ image. This difference could be as large as

500 m in the case of the 1-km bands of MODIS. Examination of the ETM+ imagery indicates that this uncertainty is less than 2% for all bands with the largest difference in the shortwave infrared bands.

The final source of uncertainty is the derivation of the surface reflectance used in computing the predicted at-sensor radiance for the 1-km<sup>2</sup> area. Past error analysis work has shown that the accuracy of the surface reflectance retrieval of the 80 m × 300 m area is 2%. Examination of Table II shows that the predicted surface reflectance of the 1-km<sup>2</sup> area differs from 2% to 5% from the measured values. This difference is a combination of the errors in the surface reflectance retrieval of the 80 m × 300 m area, the atmospheric correction of the ETM+ data (including possible biases), the curve fit method to the surface reflectance, and the sampling errors of the ground-based measurements. These errors represent a worst case source of error because we are considering the absolute error in reflectance. However, the absolute error in reflectance is not as important as band to band errors in the spectral reflectance. This is because the curve fit approach to the atmospherically corrected ETM+ data keeps the same spectral shape of the surface and simply forces this to match the ETM+ results. The band-to-band precision of the retrieved reflectance is difficult to assess at this stage of the research since this precision depends on the band-to-band characteristics of

the ground-based spectrometers, the spatial heterogeneity of the spectral reflectance of the test site, the uncertainty in the curve fit approach, and possible band-to-band biases in ETM+. All of these factors are currently under study but it is reasonable to expect that the largest difference of 5% seen in Table II will not be exceeded and it should be possible to achieve better than 2%.

Based on the above discussion, it is clear that the primary source of uncertainty is the derived surface reflectance. If all errors are assumed to be independent (and this remains to be shown), then a root-sum-square gives uncertainties in the current approach to be greater than 2.4% and no worse than 5.2%. Because this approach relies primarily on relative comparisons between sensors, it should be feasible to improve on the 2.4% value for sensors that are close in time with similar geometry. For example, cross comparison of ALI and Hyperion over a site such as Railroad Valley could have uncertainties less than 1% for ALI bands in the NIR.

## VI. CONCLUSION

The results of a cross-calibration approach between the solar reflective bands of ALI, ETM+, Hyperion, Ikonos, and MODIS show that all of the sensors agree to better than 5% (except for bands 2 and 3 of Ikonos), and this is within the uncertainties of the approach. The method relies on using the ETM+ data to compute the spectral reflectance of a selected region of the Railroad Valley Playa. This reflectance is used as input to a radiative transfer code along with ground-based measurements of atmospheric properties at the time of the overpass of the other sensors. The results shown here indicate the utility of the cross-calibration approach and the use of Railroad Valley Playa. Especially good agreement is found between ALI, ETM+, and MODIS with differences that are less than 2.3% in all bands in the visible and NIR. Slightly larger differences are seen in the shortwave infrared and work is underway to understand the cause of the larger differences in these bands. However, the agreement is still better than 4.4%, indicating that these three sensors agree to well within their combined uncertainties in radiometric calibration.

Agreement between ETM+ and Hyperion is poorer. Part of this appears to be due to low signal-to-noise in the Hyperion sensor as a result of the high spectral resolution. This can be seen in the fact that the percent difference between the two sensors does not change smoothly with wavelength as would be expected. A portion of this effect can be due to the spectral registration between the predicted radiance and the sensor radiance. This effect is dominant in regions of atmospheric absorption and is most likely the primary cause of the effects seen in the SWIR portion of the spectrum. Averaging of the Hyperion results as a function of wavelength reduces the difference between ETM+ and Hyperion, and averages over 50-nm intervals lead to differences within 6.4% of ETM+ for all bands between 500 and 900 nm with a significant portion of the spectrum having less than 3% differences. Poorer agreement is still found in the shortwave infrared as with the other sensors, but this is exacerbated by atmospheric absorption.

Future work will examine the possibility of applying this approach to dates for which there are coincident imagery data but

for which there is no coincident atmospheric data or surface reflectance data. In addition, the location of the ASTER and MISR on the Terra platform offer additional opportunities for cross calibration between the sensors used here. Applying the cross-calibration approach to a larger area of the playa should reduce uncertainties due to misregistration; however, spatial-spectral analysis of the playa using data from hyperspectral airborne sensors will evaluate whether this will be the case or whether the use of a larger portion of the playa will lead to biases in the ETM+ based surface reflectance. With the current trend toward multiple sensors and multiple platforms working toward common datasets, it will be critical to ensure that the data from these sensors are consistent. This consistency is especially crucial when attempting to extend the useful dataset of terrestrial remote sensing backward in time to include the early Landsat sensors and forward in time to include future sensors for terrestrial imaging.

## ACKNOWLEDGMENT

The authors wish to acknowledge the help of the EO-1 team at Goddard Space Flight Center for their help in receiving the EO-1 data used here (especially S. Ungar, L. Ong, and T. Brakke), the ALI team at MIT Lincoln Laboratory for their help with the calibration of the ALI data (especially D. Lencioni and J. Mendenhall), and the Hyperion team at TRW (especially P. Jarecke and J. Pearlman) for their help in understanding the Hyperion data. The authors also wish to acknowledge the help of the Bureau of Land Management office in Tonopah, NV, for their assistance in accessing the Railroad Valley test site used in this work and the assistance of numerous people in their help with collecting the ground-based data used here. Additionally, they would like to thank the reviewers for their diligence and effort leading to a greatly improved paper.

## REFERENCES

- [1] W. A. Hovis, J. S. Knoll, and G. R. Smith, "Aircraft measurements for calibration of an orbiting spacecraft sensor," *Appl. Opt.*, vol. 24, pp. 407–410, 1985.
- [2] Y. J. Kaufman and B. N. Holben, "Calibration of the AVHRR visible and near-IR bands by atmospheric scattering, ocean glint, and desert reflection," *Int. J. Remote Sens.*, vol. 14, pp. 21–52, 1993.
- [3] E. Vermote, R. P. Santer, P. Y. Deschamps, and M. Herman, "In-flight calibration of large field of view sensors at short wavelengths using Rayleigh scattering," *Int. J. Remote Sens.*, vol. 13, pp. 3409–3429, 1992.
- [4] G. Vane, R. O. Green, T. G. Chrien, H. T. Enmark, E. G. Hansen, and W. M. Porter, "The Airborne Visible/Infrared Imaging Spectrometer (AVIRIS)," *Remote Sens. Environ.*, vol. 44, pp. 127–143, 1993.
- [5] K. Thome, B. Markham, J. Barker, P. Slater, and S. Biggar, "Radiometric calibration of Landsat," *Photogramm. Eng. Remote Sensing*, vol. 63, pp. 853–858, 1997.
- [6] P. N. Slater, S. F. Biggar, R. G. Holm, R. D. Jackson, Y. Mao, M. S. Moran, J. M. Palmer, and B. Yuan, "Reflectance- and radiance-based methods for the in-flight absolute calibration of multispectral sensors," *Remote Sens. Environ.*, vol. 22, pp. 11–37, 1987.
- [7] S. F. Biggar, P. N. Slater, and D. I. Gellman, "Uncertainties in the in-flight calibration of sensors with reference to measured ground sites in the 0.4 to 1.1  $\mu\text{m}$  range," *Remote Sens. Environ.*, vol. 48, pp. 242–252, 1994.
- [8] P. N. Slater, S. F. Biggar, J. M. Palmer, and K. J. Thome, "Unified approach to pre- and in-flight satellite sensor absolute radiometric calibration," *Proc. SPIE*, vol. 2583, pp. 130–141, 1995.

- [9] P. M. Teillet, P. N. Slater, T. Ding, R. P. Santer, R. D. Jackson, and M. S. Moran, "Three methods for the absolute calibration of the NOAA AVHRR sensors in-flight," *Remote Sens. Environ.*, vol. 31, pp. 105–120, 1990.
- [10] J. L. Barker, S. K. Dolan, P. A. Sabelhaus, D. L. Williams, J. R. Irons, B. L. Markham, J. T. Bolek, S. S. Scott, R. J. Thompson, J. J. Rapp, T. J. Arvidson, J. F. Kane, and J. C. Storey, "Landsat-7 mission and early results," in *Proc. SPIE*, vol. 3870, 1999, pp. 299–311.
- [11] K. Thome, E. Whittington, J. LaMarr, N. Anderson, and P. Nandy, "Early ground-reference calibration results for Landsat-7 ETM+ using small test sites," *Proc. SPIE*, vol. 4049, pp. 134–142, 2000.
- [12] K. J. Thome, J. H. LaMarr, S. F. Biggar, and A. S. Lopez, "Ground-reference calibration of Landsat-7 ETM+," *Proc. SPIE*, vol. 3870, pp. 234–242, 1999.
- [13] J. J. Butler and R. A. Barnes, "Calibration strategy for the Earth Observing System (EOS)-AM1 platform," *IEEE Trans. Geosci. Remote Sensing*, vol. 36, pp. 1056–1061, July 1998.
- [14] W. L. Barnes, T. S. Pagano, and V. V. Salomonson, "Prelaunch characteristics of the Moderate Resolution Imaging Spectroradiometer (MODIS) on EOS-AM1," *IEEE Trans. Geosci. Remote Sensing*, vol. 36, pp. 1088–1100, July 1998.
- [15] K. P. Scott, K. J. Thome, and M. R. Brownlee, "Evaluation of the Railroad Valley playa for use in vicarious calibration," *Proc. SPIE*, vol. 2818, 1996.
- [16] E. E. Whittington, K. J. Thome, R. A. Barnes, and K. A. Canham, "Radiometric calibration of the sea-viewing wide field of view sensor using ground-reference techniques," *Proc. SPIE*, vol. 4135, pp. 294–301, 2000.
- [17] P. M. Teillet, G. Fedosejevs, R. P. Gauthier, N. T. O'Neill, K. J. Thome, S. F. Biggar, H. Ripley, and A. Meygret, "A generalized approach to the vicarious calibration of multiple Earth observation sensors using hyperspectral data," *Remote Sens. Environ.*, vol. 77, pp. 304–327, 2001.
- [18] A. R. Ehsani, J. A. Reagan, and W. H. Erxleben, "Design and performance analysis of an automated 10-channel solar radiometer instrument," *J. Atmos. Oceanic Technol.*, vol. 15, pp. 697–707, 1998.
- [19] D. I. Gellman, S. F. Biggar, P. N. Slater, and C. J. Bruegge, "Calibrated intercepts for solar radiometers used in remote sensor calibration," *Proc. SPIE*, vol. 1493, pp. 19–24, 1991.
- [20] S. F. Biggar, D. I. Gellman, and P. N. Slater, "Improved evaluation of optical depth components from Langley plot data," *Remote Sens. Environ.*, vol. 32, pp. 91–101, 1990.
- [21] K. J. Thome, B. M. Herman, and J. A. Reagan, "Determination of precipitable water from solar transmission," *J. Appl. Meteorol.*, vol. 31, pp. 157–165, 1992.
- [22] B. M. Herman and S. R. Browning, "A numerical solution to the equation of radiative transfer," *J. Atmos. Sci.*, vol. 22, pp. 559–566, 1965.
- [23] A. Berk, L. S. Bernstein, and D. C. Robertson, "MODTRAN: A moderate resolution model for LOWTRAN7," Phillips Lab., Geophysics Directorate, Hanscom AFB, MA., Tech. Rep. GL-TR-90-0122, 1989.
- [24] K. Thome, E. Whittington, N. Smith, P. Nandy, and E. Zalewski, "Ground-reference technique for the absolute calibration of MODIS," *Proc. SPIE*, vol. 4135, pp. 51–59, 2000.

- [25] S. Unger, "Ground-reference technique for the absolute calibration of MODIS," *IEEE Trans. Geosci. Remote Sensing*, vol. 38, pp. 51–59, Jan. 2000.



**Kurtis J. Thome** received the B.S. degree in meteorology from Texas A&M University, College Station, and the M.S. and Ph.D. degrees in atmospheric sciences from the University of Arizona, Tuscon.

He is currently an Associate Professor of optical sciences at the University of Arizona, where he is the head of the Remote Sensing Group. He has served as a member of the Landsat-7, ASTER, and MODIS science teams. His current research is focused on the vicarious calibration of earth-imaging sensors and related studies in atmospheric remote sensing, radiative transfer, and satellite atmospheric correction.



**Stuart F. Biggar** received the B.S. and M.S. degrees in physics from the United States Air Force Academy, Colorado Springs, CO, and The Ohio State University, Columbus, respectively. He received the M.S. and Ph.D. degrees in optical sciences from the Optical Sciences Center, University of Arizona, Tuscon.

He is currently a Research Professor of optical sciences at the University of Arizona, working in the Remote Sensing Group. His current research includes radiometry, radiometric calibration of optical systems, diffuse reflectance measurements, and vicarious calibration of optical sensors.



**Wit Wisniewski** received B.S. degree in electrical engineering, in 1980, and the M.S. degree in electrical and computer engineering, in 1991, both from the University of Arizona, Tuscon. He is currently pursuing the Ph.D. degree in electrical and computer engineering, and remote sensing and spatial analysis at the University of Arizona.

From 2000 to 2003, he was a Research Assistant in the Remote Sensing Group, Optical Sciences Center, University of Arizona.